ISSN: 2148-9173 **Vol: 9 Issue:4 December 2022**

International Journal of Environment and Geoinformatics (IJEGEO) is an international, multidisciplinary, peer reviewed, open access journal.

SST Correlation Between Chlorophyll and Turbidity by Landsat MS Image Analysis for the Coast of Izmir Province

Mert KAYALIK, Özşen ÇORUMLUOĞLU

Abstracting and Indexing: TR DIZIN, DOAJ, Index Copernicus, OAJI, Scientific Indexing Services, International Scientific Indexing, Journal Factor, Google Scholar, Ulrich's Periodicals Directory, WorldCat, DRJI, ResearchBib, SOBIAD

International Journal of Environment and Geoinformatics 9(4): 035-045 (2022)

Research Article

SST Correlation Between Chlorophyll and Turbidity by Landsat MS Image Analysis for the Coast of Izmir Province

Mert Kayalık*, Özşen Çorumluoğlu

Department of Geomatics Engineering, Faculty of Engineering and Architecture, İzmir Katip Çelebi University, İzmir, TURKIYE

* Corresponding author: M. Kayalık
e-mail: mert.kayalik@ikcu.edu.tr

Received 31.01.2022
Accepted 14.04.2022

How to cite: Kayalık and Çorumluoğlu (2022). SST Correlation Between Chlorophyll and Turbidity by Landsat MS Image Analysis for the Coast of Izmir Province. *International Journal of Environment and Geoinformatics (IJEGEO)*, 9(4): 035-045. doi. 10.30897/ijegeo.1065482

Abstract

Temporal Sea Surface Temperature (SST) analyses by satellite images are quite vital in terms of understanding the sea water quality. Specific water quality criteria include dissolved oxygen, chlorophyll, temperature, depth, pH, salinity, and turbidity, and these criteria are used to determine water quality in seas. In the current study, three criteria which are chlorophyll, temperature (SST) and turbidity were examined through their correlation with SST derived from Landsat sensors. This let to know about the examined criteria at minimum and maximum temperature dates, the relation with respect to temperature change rates, and to understand the events that occur in certain dates. The regular or irregular increases of the detected SST are evidence of sea water quality or pollution resulted from the criteria in the study area. Therefore, first turbid water which contains a high amount of suspended sediment was studied. After the turbidity index was completed, the Chlorophyll study was carried out to detect the algae like substances. The aims of the study are to evaluate the temporal change of water quality in coastal region of Izmir province, using spectral indices, and to contribute to the development of more sensitive qualitative index algorithms in the future. The purpose of the correlation analysis performed after the indices are processed is to show that the SST and index results are compatible with each other. At the end of the study, high correlation coefficients revealed the positive relationship between SST and indices.

Keywords: Landsat Satellite, Sea Surface Temperature, Turbidity, Chlorophyll

Introduction

We know that sea surface temperature data was collected by in situ measurements with ships in the past, nowadays we can acquire such data through Remote Sensing technology without going to study area (Thomas et al., 2002). LANDSAT sensors acquire surface temperature data and store it as Digital Numbers (DNs) (Tarantino, 2012). The thermal bands of the Landsat satellite are used to estimate the water temperature (Xing et al., 2006). Thermal bands differ according to the band combination of each satellite, while the thermal band is sixth band (10.4 – 12.5µm) for Landsat 5, it is known as tenth (10.6 – 11.19µm) and eleventh (11.5 – 12.51µm) band for Landsat 8. The resulting SST data represent the skin temperature of the water which is less than 1 mm of the uppermost water layer (Xing et al., 2014). SST output maps also provide answers to some questions; 'Does the region has a consistent feature of SST climatology?', 'Is there a homogeneous SST?' (Tarantino, 2012). At the end of the study, a regression analysis examining the correlation equation and correlation coefficient should be performed to look at the correlation (relationship) of the SST with other indices. The fact that the mentioned correlation coefficient is close to 1 is proof that the study was conducted with consistent indices.

One of the main contributions of this study is to provide an understanding of the definition of "clean surface clean bottom" for all seas. What is meant by this definition is that sea surface information gives us some ideas about the situation under the sea. In other words, sea surface temperature allows us to see the big picture under the sea. In addition to all these, since marine pollution lowers dissolved oxygen, life in the water changes and a large number of sea creatures are negatively affected, and may even die (Alshaikh, 2016). The irregularity of these deaths is closely related to serious issues such as the extinction of sea creatures. Wastewater and dirt that results as decrease of dissolved oxygen level in sea cause a noticeable increase in sea surface temperature (SST). Unfortunately, many aquatic organisms are very sensitive to small temperature changes as little as one degree Celsius (Alshaikh, 2016). In addition, as the sea temperature increases, the evaporation rate also increases, which causes more water wastage and condensed mineral contents in sea water (Tarantino, 2012).

As suspended particles in the water increase, the turbidity level of the water also increases. Increasing turbidity causes the red band to reflect more than the green band (Rahman et al., 2011). These bands and combinations are regularly used to detect turbidity and suspended sediments in water bodies (Baughman et al., 2015). Turbidity Indices allow detection of high turbidity (low clarity) water cover information (Gardelle et al., 2010). Turbidity has a correlation with suspended matter as water turbidity is a sign of sedimentation processes.

They create a fruitful environment for chlorophyll (Lai et al., 2021). Therefore, chlorophyll prediction is considered an indication of the nutritional status of the water body (Patra et al., 2016). Chlorophyll in water is an important indicator of phytoplankton biomass (Tepanosayn et al., 2017; Gazi,oğlu, 2018). The presence of phytoplankton in the sea causes selective absorption of light by chlorophyll-pigment and causes the color of the sea to change. In addition, chlorophyll-a concentrations are indicators of algae biomass (Tan et al., 2017; Acar et al., 2021). One of the primary concerns for all is the algae bloom in the seas. Therefore, understanding of Chlorophyll is critical for marine life (Gazioğlu, et al., 2022).

Therefore, the aim of this study was to reveal the impact of human activities in the Aegean coastal sea regions close to the coasts of Aliağa and İzmir. Such activities can increase sea temperatures and turbidity in the region. The study analyzes these conditions in focused regions of the Aegean Sea using Remote Sensing Techniques. As it can be understood, since it creates pollution by reducing the amount of oxygen in sea water, the increase in temperature and turbidity in the sea triggers the increase of chlorophyll-a, which creates a productive environment for harmful marine plants to grow. Therefore, it is important to temporarily monitor these variables in order to keep our marine resources safe and sustainable. The temporal analyzes made possible by Remote Sensing and used here in this study are superior to other classical in situ techniques as they rely on labour-intensive fieldwork.

Materials and Methods

Data acquisition

Landsat satellite data can be downloaded from the Earth Explorer USGS site at no cost. In addition, path / row information can be entered to quickly access the study area. The path / row value of current study area is 181/33. For the sake of clearer and cloudless satellite images it was preferred to download images with 'less than 10% cloud cover'. Downloading satellite images from the summer months when the sky is the cleanest will provide a more sensitive study (Xing et al., 2014). In the study, totally 8 satellite images were downloaded between 1998-2018. As shown in Table 1, five satellite images were obtained as Landsat 5 and three satellite images as Landsat 8 data. Data properties which is valid for all images are Image Quality: 9, Map Projection: UTM, Map Datum: WGS84, Map Ellipsoid: WGS84, Pixel Size: 30×30. Details of the satellite images are available in Table 1.

Table 1. Data acquisition dates of Landsat 5 and Landsat 8 satellites with the same path/row information.

Data Dates	Data Type	Spacecraft ID	Sensor ID	Path/ Row
July 28, 1998	LT05	Landsat 5	TM	181/33
July 20, 2001	LT05	Landsat 5	TM	181/33
August 13, 2004	LT05	Landsat 5	TM	181/33
August 22, 2007	LT05	Landsat 5	TM	181/33
August 14, 2010	LT05	Landsat 5	TM	181/33
August 6, 2013	LC08	Landsat 8	OLI	181/33
July 13, 2016	LC08	Landsat 8	OLI	181/33
July 3, 2018	LC08	Landsat 8	OLI	181/33

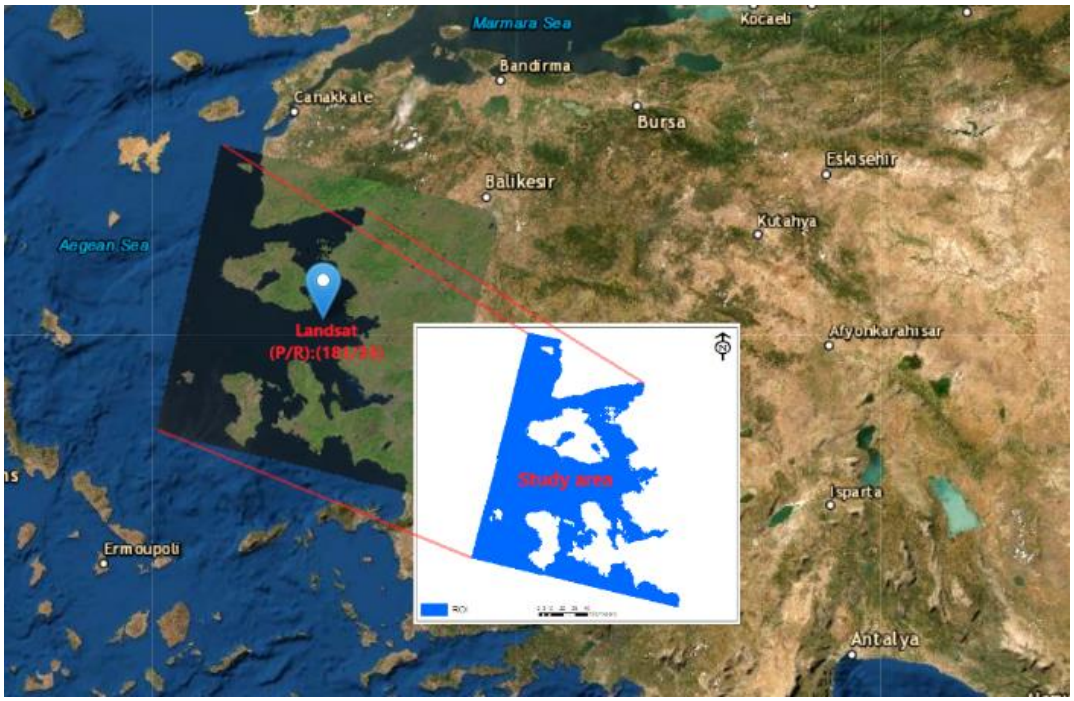

Fig. 1: Study area with Earth Explorer USGS basemap.

Study area

Section of the Aegean Sea between 41° - 35° north latitudes, and 23° - 27°/ 28 ° east longitude was selected as study area. It is approximately 660 km long from north to south; its width is 270 km in the north, 150 km in the middle and 400 km in the south. The surface area of the Aegean Sea, which joins to the Marmara Sea and the Black Sea through the Dardanelles, is about 214,000 km^2. The Aegean Sea is ranked third in size in the seas surrounding Turkey. It is the main way for petroleum products transported over the Black Sea to reach the world market. The Aegean Sea reaches to the Mediterranean Sea at the south, and extends to the shores of the two countries at the east and west respectively, Turkey and Greece. There are quite a number of islands and islets in the Aegean Sea. Sea water temperatures generally increase from north to south. This increase is more pronounced in winter. Although the Aegean Sea is rich in oxygen, it is poor in phosphate and nitrate. The study area in the Aegean Sea, where scientific research has intensified on sea pollution and other issues, is shown as in Figure 1.

Data Processing

Computation of SST (in Celsius)

Thermal bands consist of Digital Number (DN) values because satellite images store analog physical values (temperature, color, etc.) as Digital Numbers (DN) to minimize storage volume (Alshaikh, 2016). It is necessary to create a model to convert these DNs in thermal image to Temperature values and here this model is designed with the Model Maker tool in ERDAS Imagine software.

The conversion of DN values to temperature values can be completed with following three-step conversion;

- -Digital Number to Radiance,
- -Radiance to Brightness Temperature,
- -Conversion from Kelvin Degree into Celsius Degree,

Finally, if it is necessary, Cloud removal and Cloud Shadow Mask processes should be followed.

Conversion from Digital Number to Radiance

The formula used for Landsat 5 is as follows;

$$L\lambda = ((LMAX\lambda - LMIN\lambda) / (QCALMAX - QCALMIN)) \times (QCAL - QCALMIN) + LMIN\lambda \quad \text{(Eq.1)}$$

where Lλ: cell value as radiance
QCAL: digital number
QCALMIN: minimum quantized calibrated pixel value
QCALMAX: maximum quantized calibrated pixel value
LMINλ: spectral radiance scales to QCALMIN
LMAXλ: spectral radiance scales to QCALMAX.

In Landsat 8, gain and bias values are used to convert DN to radiance;

$$L\lambda = gain \times DN + bias \quad \text{(Eq.2)}$$

where Lλ: cell value as radiance
DN: cell value digital number
gain: gain value for a specific band
bias: bias value for a specific band.

Conversion Radiance into Brightness Temperature

Radiance should be converted to brightness temperature using the thermal constants in the Metadata file (MTL file) that is downloaded with the Satellite images (Corumluoglu & Asri, 2015),

$$T = K2 / \ln ((K1 / L\gamma) + 1) \quad \text{(Eq.3)}$$

where T: brightness temperature in Kelvin
K1 and K2: thermal conversion constant
L_γ: radiance value.

MTL file showing some details (mission and calibration details) and expressions (radiance, reflectance, and temperature expressions) of satellite images can be examined with Landsat Tools V1.0.34 software. Equations (1), (2), and (3) describe which mathematical parameters the model uses in the background to convert DN values to temperature values. Celsius value can be obtained by subtracting 273.15 °K from the result. ArcMap 10.4 software was used to color the sea surface temperature (in Celsius) results. Images whit many information, such as temperature variations between years, places with high and low temperatures, are shown in Figure 2.

Indices

Index methods are mostly used for several purposes on surface water estimations which they separates the water quality contents from background noises and threshold values can then be used for highlighting (Acharya et al., 2017). Two types of indices were used in this study; the first one is for turbidity, and the second is for chlorophyll. The most important part in this process is obtaining the reflectance values (Corumluoglu, 2021).

The conversion of DN values to reflectance values can be completed in these three steps;

- -Conversion from Digital Number to Radiance,
- -Conversion from Radiance to Top of Atmosphere (ToA) Reflectance
- -Conversion from Top of Atmosphere (ToA) Reflectance to surface reflectance

Finally, if it is necessary, Cloud removal and Cloud Shadow Mask processes should be followed.

The 'DN to Radiance' conversion step is similar with the step described in the ‘Computation of SST’ section. Landsat 8 can also be converted directly to the Top of Atmosphere (ToA) reflectance value without calculating radiance. Therefore, there is no "DN to Radiance" conversion step for Landsat 8.

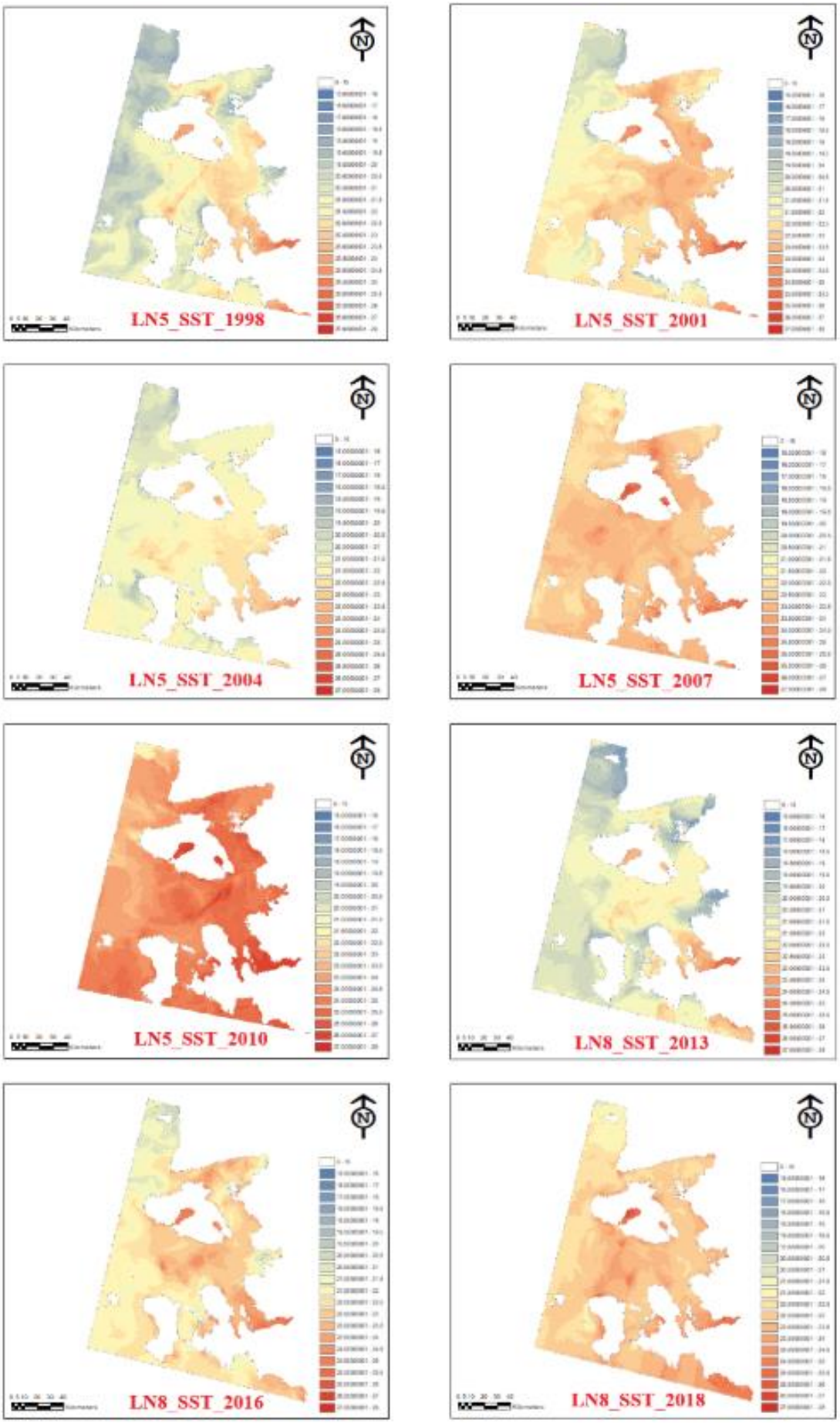

Fig. 2: SST maps within the range of min. 15 and max. 28 degrees.

Conversion from Radiance to ToA Reflectance

The formula used for Landsat 5 is as follows;

$$\rho\lambda = \pi \times L\lambda \times ((d\text{^}2) / ESUN_{\lambda}) \times \cos\Theta s \qquad \text{(Eq. 4)}$$

where ρλ: Unitless planetary reflectance
Lλ: spectral radiance
d: Earth-Sun distance in astronomical units
$ESUN_{\lambda}$: mean solar exoatmospheric irradiances
Θs: solar zenith angle.

In Landsat 8, DN's can be converted to ToA reflectance using the rescaling coefficients;

$$\rho\lambda\imath = M\rho \times Qcal + A_{\rho} \qquad \text{(Eq. 5)}$$

where ρλı: ToA planetary reflectance without correction for solar angle
Mρ: Band-specific multiplicative rescaling factor
A_{ρ} : Band-specific additive rescaling factor
Qcal: Quantized and calibrated standard product pixel values (DN).

ToA reflectance with a correction for the sun angle is;

$$\rho\lambda = \rho\lambda\imath / \cos(\theta sz) \qquad \text{(Eq. 6)}$$

where ρλ: ToA planetary reflectance
cos(θsz): Local solar zenith angle.

Equations (4), (5) and (6) describe which mathematical parameters are introduced into the model to convert the DN values to ToA reflectance values.

Conversion continued with Dark Object Subtraction model to remove the atmospheric effect from the reflectance values, which must be done for each band individually to obtain the surface reflectance values. The Dark Object Subtraction (DOS) method is an image-based technique to cancel out the haze and mist component caused by additive scattering from remote sensing data (Chavez, 1988). Dark object subtraction depends on searching each band for the darkest pixel value to subtract that values from ToA values of each pixel in the whole scene (Boucher et al., 2018).
Unfortunately, since two thirds of the earth's surface always covered by cloud every year (Wang et al., 1999), the cloud and cloud shadow on the study area means that it greatly reduces the number of available pixels (Candra et al., 2016). There are many techniques to solve this problem;

- -Multi temporal Cloud Masking (MCM),
- -QA band (Landsat quality assessment band),
- -Automated Cloud-Cover Assessment (ACCA),
- -Function of Mask (Fmask),
- -Multi Temporal mask (Tmask).

In the current study, Fmask method which uses the difference reflectance values between clear pixels and cloud and cloud shadow pixels was selected. In this approach, cloud physical properties are used to distinguish between Potential Cloud Pixels (PCPs) and cloud free area (Zhu and Woodcock, 2012). However, there are several drawbacks of Fmask (Candra et al., 2016). Firstly, Fmask tends to fail to detect cloud which is warm and thin. Secondly, Fmask tends to classify very bright and cold land such as cold snow as cloud. Consequently, SST and Index studies were carried out with cloudless images. An example of removing the cloud and cloud shadows from each band is given in Figure 3.

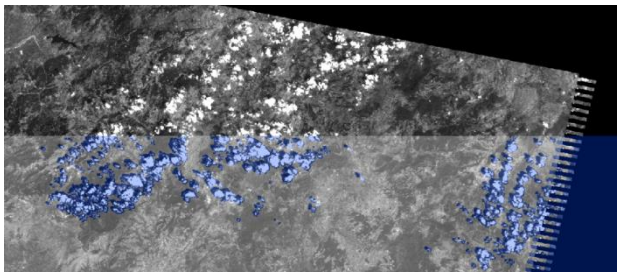

Fig. 3: Elimination of cloud and cloud shadows through ArcGIS 10.4 software.

Computation of indices
The term "Remote Sensing," describes the use of indices to make discernments about environmental phenomena. All Spectral indices are used in remote sensing to identify a particular surface-cover type based upon its absorption or reflection of incident solar energy in different regions of the electromagnetic spectrum (Cole et al., 2015). Over the years numerous spectral indices have been introduced by the scientific community to solve complex environmental (or other) issues. Indices and band ratios are the most common form of spectral enhancement.

Normalized Difference Turbidity Index (NDTI)
Turbidity indices use spectral reflectance values which increase with increasing turbidity in the concern of water bodies. It is also known that the turbidity level of the water increases as the particles suspended in the water increase. NDTI is one of the algorithms developed to evaluate the turbidity level of open water. The band formula given in equation (7) is regularly used to detect turbidity (Subramaniam, S.; Saxena, 2011).

$$NDTI = - ((red - green) / (red + green)) \qquad \text{(Eq. 7)}$$

where red and green spectral bands: correspond to Band 3 (0.63 - 0.69μm) and Band 2 (0.53 - 0.61μm) for Landsat 5 TM while Band 4 (0.63 - 0.68μm) and Band 3 (0.53 - 0.60μm) for Landsat 8 OLI.

As a result of processing the formula mentioned in equation (7), the output maps in Figure 4 were obtained. All maps show turbidity index results between -1 and +1. All presented maps were created by setting up a model using turbidity index formula given in equation 7 via Model maker in Erdas Imagine software.

Chlorophyll-a Index

Chlorophyll-a is a photosynthetic pigment found in all green flower components, including algae and cyanobacteria (O'Reilly et al., 2019; Tan et al., 2017). Many band combinations and developed algorithm can be used to estimate chlorophyll-a concentration (Boucher et al., 2018; Tangx et al., 2021). Normalized Difference Vegetation Index (NDVI) can also be used to detect suspended sediments in water bodies, but in this study area, the Kab-1 algorithm, which gives the best results for chlorophyll detection and has a high correlation coefficient with SST, was used (Brandon et al., 2021). The Kab-1algorithm formula that gives the chlorophyll index can be used as follows (Boucher et al., 2018).

$$Kab\_1 = 1.67 - 3.94 \times \ln(blue) + 3.78 \times \ln(green) \quad \text{(Eq.8)}$$

where blue and green spectral bands: correspond to Band 1 (0.45 - 0.52µm) and Band 2 (0.53 - 0.61µm) for Landsat 5 TM while Band 2 (0.45 - 0.52µm) and Band 3 (0.53 - 0.60µm) for Landsat 8 OLI.

The output maps of the 'Kab_1' algorithm, which is vital for marine life, are given in Figure 5, previous to next years respectively. As seen in Figure 5, the values on all maps for chlorophyll-a index vary between -1 and +1.

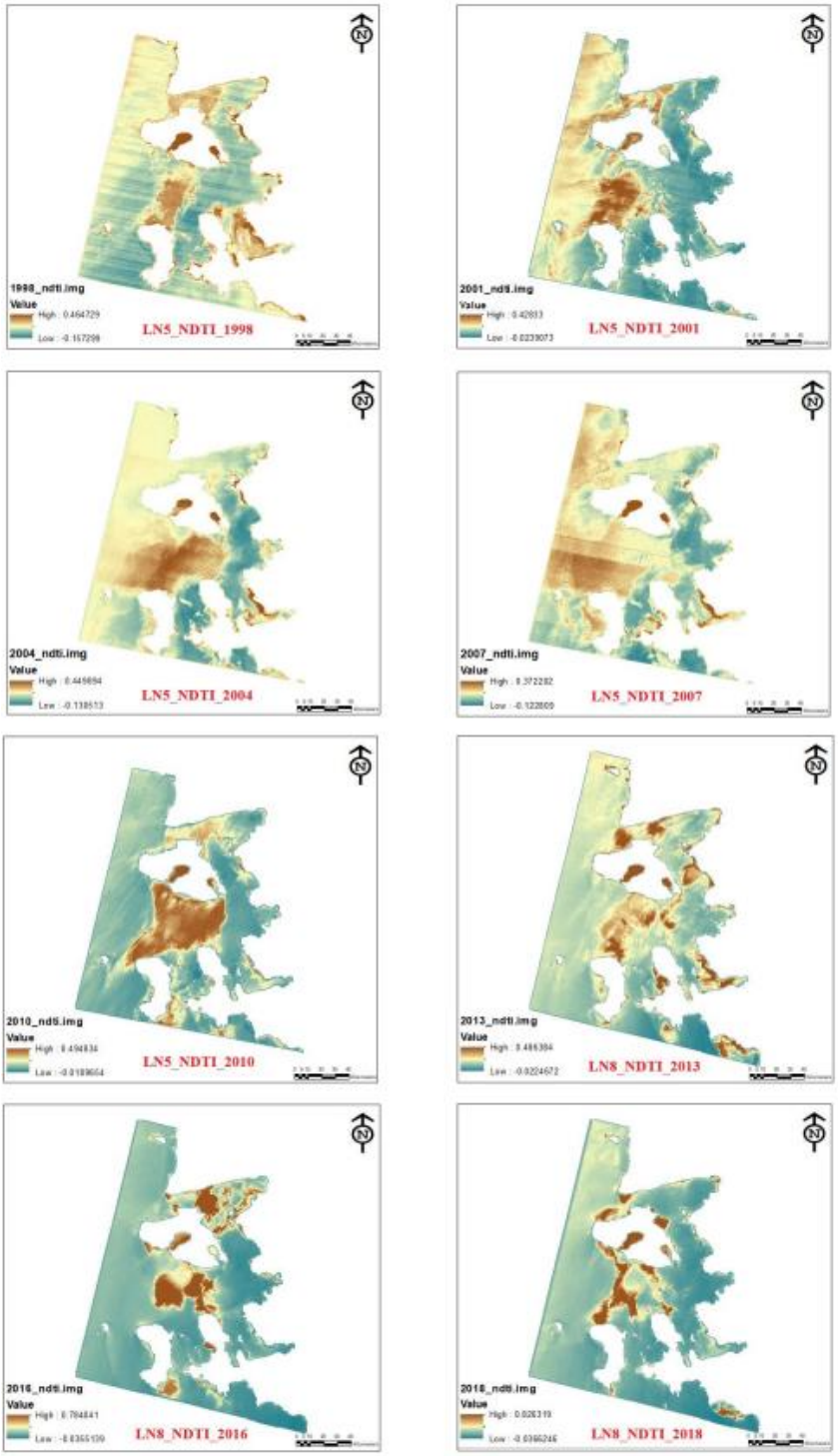

Fig. 4: Turbidity output maps.

Results and Discussion

Interpretation of SST results

When we colored the temperature data obtained in the Celsius as seen in Figure 2, high and irregular SST increases were observed due to the dense population of İzmir and the presence of industrial communities close to the gulf. High and irregular SST increase was also found in Aliağa and its surrounding, where heavy oil industry and ore factory establishments such as 'Tüpraş Inc., Petkim Inc.' and steel factories. In addition, the region between the island of Lesbos and Chios is among the regions where high and irregular SST increase are seen. It is clear that generally temperatures increase significantly when going from deep to shore. While similar comments can be made for each data in the region, an extra high sea surface temperature was detected in the 2010 image.

Examining the data on Figure 6 will enable us to better understand the results and make more accurate comments. The chart presents three basic information; minimum, maximum and average temperatures. When we look carefully at the average temperature part of the graph, the years 1998, 2010, and 2018 shared the peak in terms of sea surface temperature values while 2004, 2013 were recorded as the years with the lowest sea surface temperature information. Although all data were taken during the summer months, irregular SST jumps are indicative of an important problem. Researching the years when these differences are identified is vital for a more sustainable environment management and marine life.

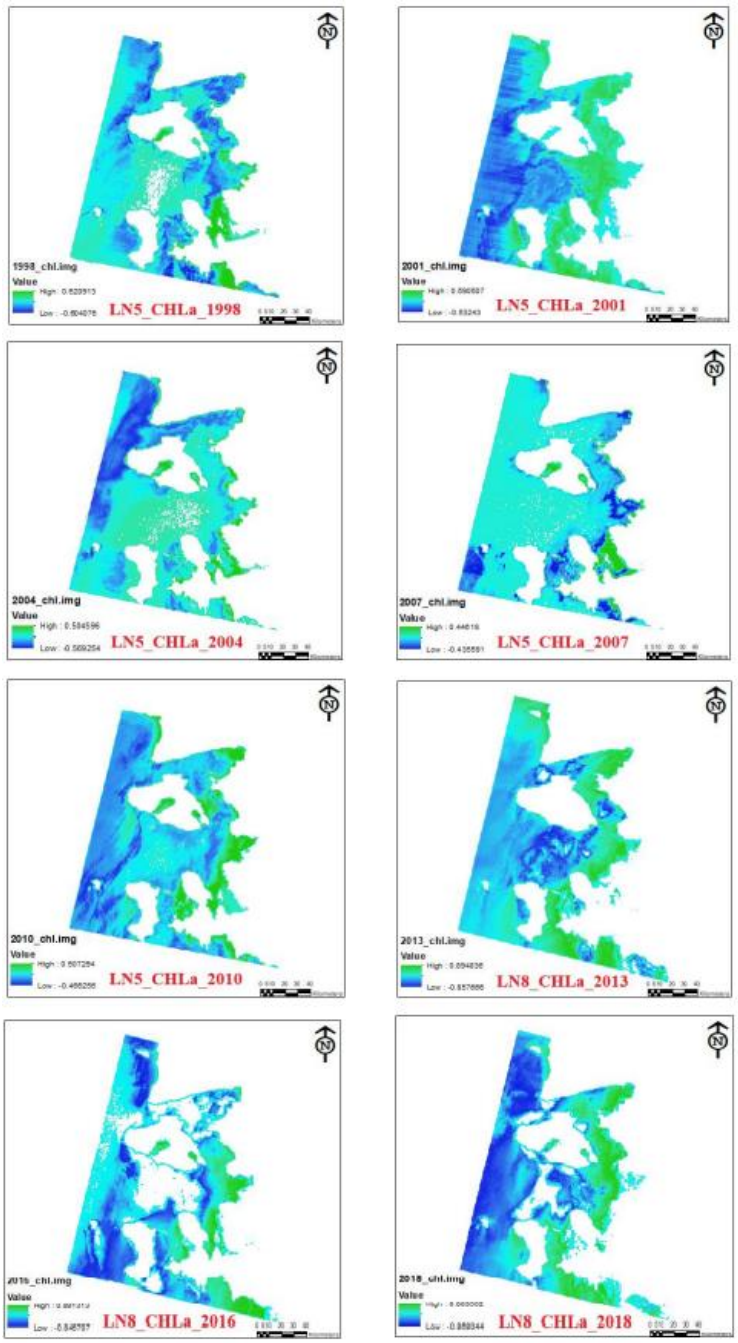

Fig. 5: Chlorophyll output maps.

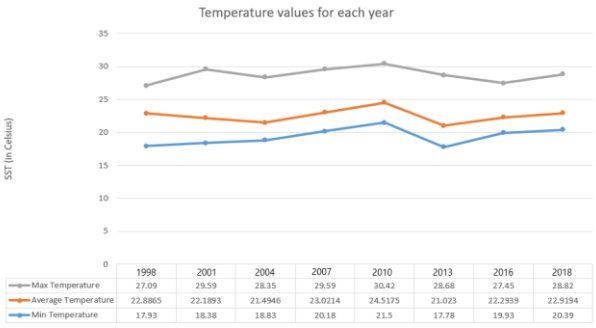

Fig. 6: Temperature changes by years.

Interpretation of Index results

When SST maps were examined against to the turbidity index result, which is among certain water quality parameters, it was noticed that the regions with regular or irregular SST increase were compatible with well-known locations in terms of pollution. As seen in Figure 4, high levels of turbidity were detected in İzmir Bay, in the region between Chios and Lesbos, and in almost all coastal areas where SST is high.

As a result of processing the formula specified in Equation (8), output maps of chlorophyll index, which is among the specific water quality parameters, were obtained. As seen in Figure 5, Kab_1 algorithm results showed that areas close to the coast are dense in terms of chlorophyll and the amount of chlorophyll decreases at the deeper regions from the coast.

"Regression analysis" was conducted in order to bring these results to a more significant level. Regression reveals the numerical relationship of two or more variables, and even making predictions. Regression analysis was used twice to see the consistency of both chlorophyll and turbidity against the SST. The graphic outputs of the regression analysis made with Excel software are shared in Figure 7 and Figure 8. Correlation coefficients revealed by regression analysis may be positive or negative. If it is zero, it indicates that there is no relationship between the two variables examined. The high correlation coefficients in Tables 2 and 3, filled with the information obtained from the graphs in Figure 7 and Figure 8, show that SST is directly related to the indices.

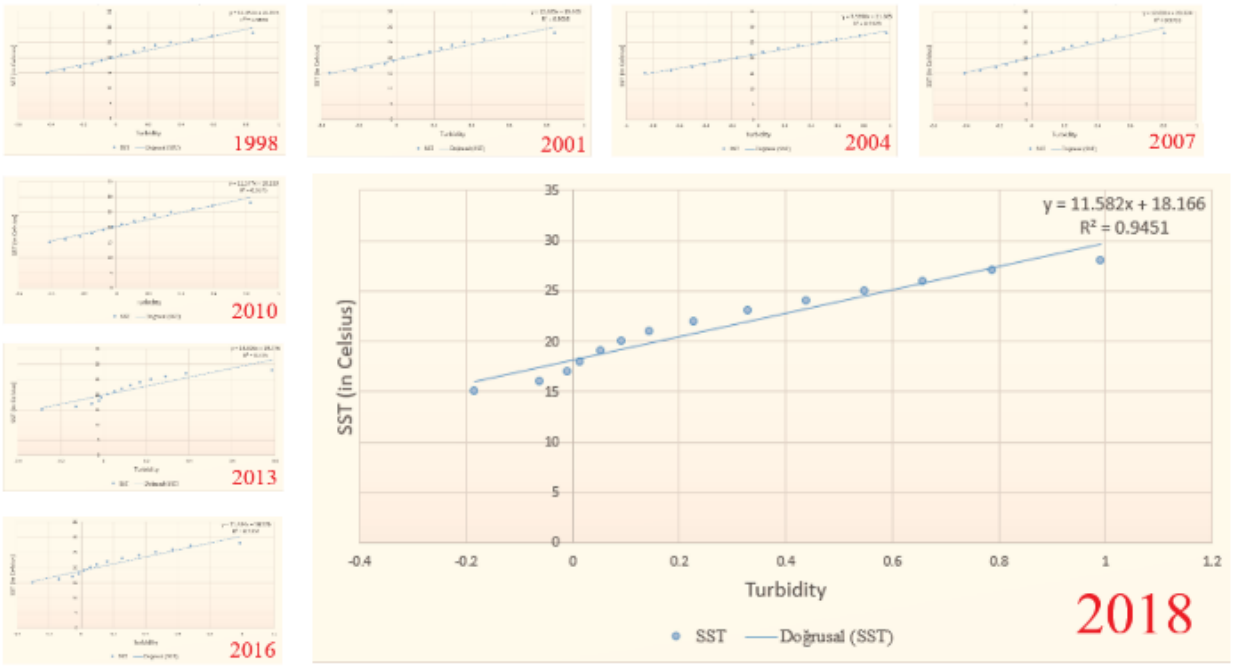

Fig. 7: Regression analysis graphics for SST and Turbidity.

Table 2: Regression analysis results between SST and Turbidity.

Data Dates	Equations	Correlation coefficients (R^2)
July 28, 1998	y = 11.453x + 20.195	0.9655
July 20, 2001	y = 12.485x + 19.405	0.9638
August 13, 2004	y = 7.5956x + 21.305	0.9929
August 22, 2007	y = 12.031x + 20.224	0.9703
August 14, 2010	y = 11.577x + 20.183	0.9675
August 6, 2013	y = 14.806x + 19.776	0.8350
July 13, 2016	y = 11.434x + 18.926	0.9334
July 3, 2018	y = 11.582x + 18.166	0.9451

The equation 'y = 11.582 x + 18.166' can also be written as 'SST = 11.582 Turbidity + 18.166'. Regression analysis results of SST and Turbidity data can be found in Table 2. While the results generally have values above 0.9, the highest correlation coefficient obtained as 0.9929 for the year 2004. The year 2013 was recorded as the year with lowest correlation coefficient with a value of 0.835. Still these values represent high correlation in general.

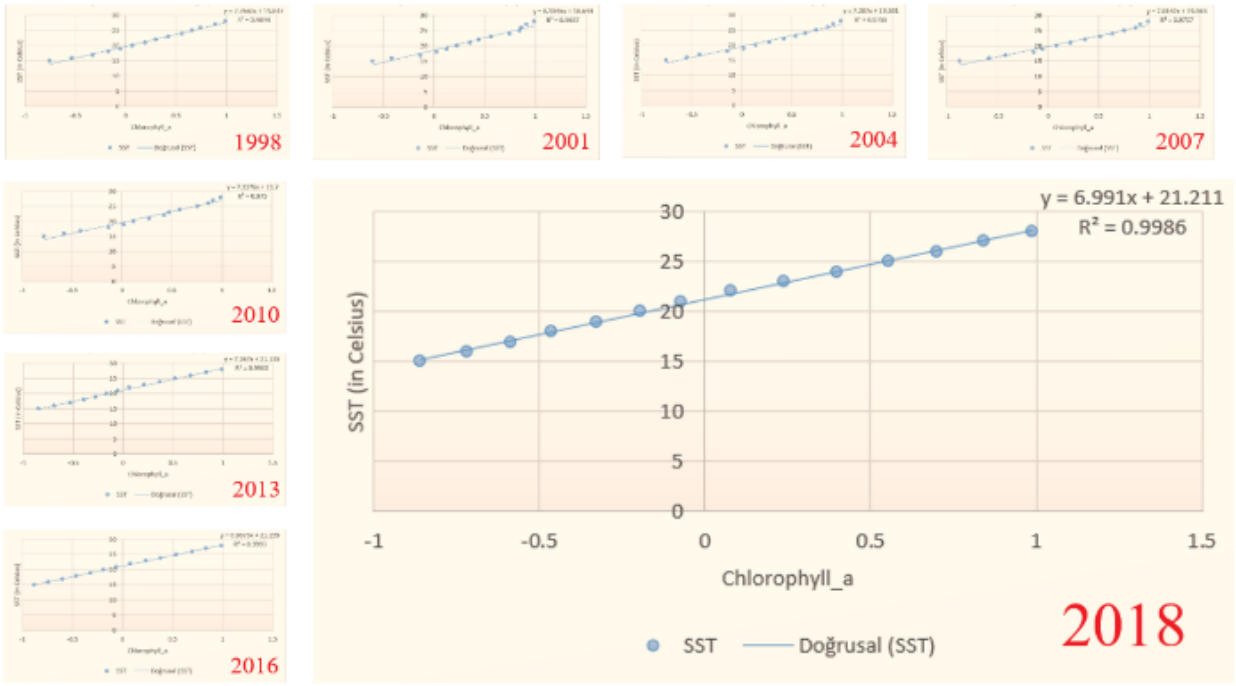

Fig. 8: Regression analysis graphics for SST and Chlorophyll.

Table 3: Regression analysis results between SST and Chlorophyll.

Data Dates	Equations	Correlation coefficients (R^2)
July 28, 1998	y = 7.7669x + 19.847	0.9894
July 20, 2001	y = 8.1046x + 18.644	0.9657
August 13, 2004	y = 7.287x + 19.6010	0.9755
August 22, 2007	y = 7.0142x + 19.866	0.9757
August 14, 2010	y = 7.2376x + 19.700	0.9750
August 6, 2013	y = 7.267x + 21.1350	0.9966
July 13, 2016	y = 6.9675x + 21.259	0.9993
July 3, 2018	y = 6.991x + 21.2110	0.9986

The equation 'y = 6.991 x + 21.211' can also be written as 'SST = 6.991 Chlorophyll + 21.211'.

Table 3 clearly shows how effective the Kab_1 algorithm works especially for Landsat 8 data and ultimately gives maximum correlation with SST. All correlation coefficients are greater than 0.95. While 2016 image showed the highest SST harmony with 0.9993 correlation coefficient, image for 2001 showed a minimum SST harmony with 0.9657 correlation coefficient. SST-Chlorophyll compatibility is higher than SST-Turbidity. But ultimately, as seen in Tables 2 and 3, positive correlation and high correlation coefficient reveal a strong relationship between SST and indices.

Conclusion

Here in this research, it is found that by the help of indices for turbidity and chlorophyll obtained from multi spectral satellite images, SST and sea water quality measures such as for turbidity and chlorophyll represented high correlations. From this point of view, it can also be concluded that many useful information in marine science can be obtained with multi spectral image analyses with remote sensing technology. The cost effective and most sensitive way to examine the status of water quality parameters is through remote sensing. Two very useful index algorithms can be run to determine the turbidity and chlorophyll similarly for other regions. In addition, the index studies allow us to understand what changes water are under and what precautions to take care of before they reach to risky levels. So, the measures can be taken efficiently by remote sensing technology to ensure a more sustainable water resource management for both the people of the environment and submarine creatures. Such analysis and studies should be carried out for a better ecosystem and human life and an environment in which useful information about water resources is available should be left to future generations.

Acknowledgements

The authors acknowledge the support of USGS, which provided the Landsat satellite imagery, and Hexagon, which produced ERDAS Imagine.

References

Acar, U., Yılmaz, O. S., Çelen, M., Ateş, A. M., Gülgen, F., Balık Şanlı, F. (2021). Determination of Mucilage in The Sea of Marmara Using Remote Sensing Techniques with Google Earth Engine. *International Journal of Environment and Geoinformatics*, 8(4), 423-434 . doi.10.30897/ijegeo.957284

Acharya, T. D., Subedi, A., Yang, I. T., Lee, D. H.

(2017). Combining Water Indices for Water and Background Threshold in Landsat Image. *Proceedings*, *2*(3), 143. doi.org/10.3390/ecsa-4-04902

Alexander A. Gilerson, Anatoly A. Gitelson, Jing Zhou, Daniela Gurlin, Wesley Moses, Ioannis Ioannou, Samir A. Ahmed (2010). Algorithms for remote estimation of chlorophyll-a in coastal and inland waters using red and near infrared bands. Opt. Express 18, 24109-24125.

Alshaikh, A. Y. (2016). *Detection of Sea Surface Temperature and Thermal Pollution of Agricultural Coastal Areas using Thermal Infrared , Jeddah City , West KSA*. *5*(1), 51–60.

Baughman, C. A., Jones, B. M., Bartz, K. K., Young, D. B., Zimmerman, C. E. (2015). Reconstructing turbidity in a glacially influenced lake using the Landsat TM and ETM+ surface reflectance climate data record archive, Lake Clark, Alaska. *Remote Sensing*, *7*(10), 13692–13710. doi.org/10.3390/rs71013692

Boucher, J., Weathers, K. C., Norouzi, H., Steele, B. (2018). Assessing the effectiveness of Landsat 8 chlorophyll a retrieval algorithms for regional freshwater monitoring. *Ecological Applications*, *28*(4), 1044–1054. doi.org/10.1002/eap.1708

Candra, D. S., Phinn, S., Scarth, P. (2016). Cloud and cloud shadow masking using multi-temporal cloud masking algorithm in tropical environmental. *International Archives of the Photogrammetry, Remote Sensing and Spatial Information Sciences - ISPRS Archives*, *41*(July), 95–100. doi.org/10.5194/isprsarchives-XLI-B2-95-2016

Chavez, P. S. (1988). An improved dark-object subtraction technique for atmospheric scattering correction of multispectral data. *Remote Sensing of Environment*, *24*(3), 459–479. doi.org/10.1016/0034-4257(88)90019-3

Cole, C. J., Friesen, B. A., Wilson, E. M., Wilds, S. R., Noble, S. M. (2015). *Use of Satellite Images to Determine Surface-Water Cover During the Flood Event of September 13 , 2013 , in Lyons and Western Longmont , Colorado*. *1258*, 20151042.

Corumluoglu, O., Asri, I. (2015). The effect of urban heat island on Izmir's city ecosystem and climate. *Environmental Science and Pollution Research*, *22*(5), 3202–3211. doi.org/10.1007/s11356-014-2874-z

Corumluoglu, O., (2021). *SSI Analysis of Long-Term UHI Development Due To Urbanization Affecting Urban Ecosystem and Local Climate Change Through City of Izmir Case*. 0–38.

Çelik, O.İ., Çelik, S. Gazioğlu, C. (2022). Evaluation on 2002-2021 CHL-A Concentrations in the Sea of Marmara with GEE enhancement of satellite data, *International Journal of Environment and Geoinformatics*, 9(4), 068-077, doi.10.30897/ijegeo. 1066168

Gardelle, J., Hiernaux, P., Kergoat, L., Grippa, M. (2010). Less rain, more water in ponds: A remote sensing study of the dynamics of surface waters from 1950 to present in pastoral Sahel (Gourma region, Mali). *Hydrology and Earth System Sciences*, *14*(2), 309–324.doi.org/10.5194/hess-14-309-2010

Gazioğlu, C. (2018). Biodiversity, Coastal Protection, Promotion and Applicability Investigation of the Ocean Health Index for Turkish Seas, International Journal of Environment and Geoinformatics, 5(3), 353-367. doi. 10.30897/ijegeo.484067.

Gazioğlu, C., Çelik Oİ., Çelik, S. (2022). Marmara Denizi için 2002-2021 Yılları Arasında Klorofil-A Değerlerinin Google Earth Engine Yardımı ile İzlenmesi, *TÜDAV Marmara Sempozyumu 2022-Istanbul* (In Turkish)

Lai, Y., Zhang, J., Song, Y., Gong, Z. (2021). Retrieval and Evaluation of Chlorophyll-a Concentration in Reservoirs with Main Water Supply Function in Beijing, China, Based on Landsat Satellite Images. International journal of environmental research and public health, 18(9), 4419. doi.org/10.3390/ijerph18094419

O'Reilly, John E., Werdell, P. Jeremy (2019). Chlorophyll algorithms for ocean color sensors - OC4, OC5 & OC6. Remote Sensing of Environment, 229, 32-47. doi.org/10.1016/j.rse.2019.04.021

Patra, P. P., Dubey, S. K., Trivedi, R. K., Suhu, S. K., Rout, S. K. (2016). Estimation of Chlorophyll-a Concentration and Trophic States for an Inland Lake from Landsat-8 OLI Data: A Case Nalban Lake of East Kalkota Wetland, India. *Preprints*, *August*, 18. doi.org/10.20944/preprints201608.0149.v1

Rahman, I. M. M., Islam, M. M., Hossain, M. M., Hossain, M. S., Begum, Z. A., Chowdhury, D. A., Chakraborty, M. K., Rahman, M. A., Nazimuddin, M., Hasegawa, H. (2011). Stagnant surface water bodies (SSWBs) as an alternative water resource for the Chittagong metropolitan area of Bangladesh: Physicochemical characterization in terms of water quality indices. In *Environmental Monitoring and Assessment* (Vol. 173, Issues 1–4). doi.org/10.1007/s10661-010-1414-7

Smith Brandon, Pahlevan Nima, Schalles John, Ruberg Steve, Errera Reagan, Ma Ronghua, Giardino Claudia, Bresciani Mariano, Barbosa Claudio, Moore Tim, Fernandez Virginia, Alikas Krista, Kangro Kersti (2021). A Chlorophyll-a Algorithm for Landsat-8 Based on Mixture Density Networks. Frontiers in Remote Sensing, 1. doi.10.3389/frsen.2020.623678

Subramaniam, S., Saxena, M. (2011). Automated Algorithm For Extraction Of Wetlands From Irs Resourcesat Liss Iii Data S.Subramaniam and Manoj Saxena RS&GIS Applications Area, National Remote Sensing Centre(NRSC), ISRO, Hyderabad, AP, 500 625, INDIA KEY WORDS: Wetland, Remote Sensing, automa. *International Archives of the Photogrammetry, Remote Sensing and Spatial Information Science, Volume XXXVIII, Part 8/W20,2011*, *XXXVIII*(November).

Tan, W., Liu, P., Liu, Y., Yang, S., Feng, S. (2017). A 30-year assessment of phytoplankton blooms in erhai lake using landsat imagery: 1987 to 2016. *Remote Sensing*, *9*(12). doi.org/10.3390/rs9121265

Tang X, Huang M. (2021). Inversion of Chlorophyll-a Concentration in Donghu Lake Based on Machine Learning Algorithm. Water, 13(9):1179. doi.org/

10.3390/w13091179

Tarantino, E. (2012). Monitoring spatial and temporal distribution of Sea Surface Temperature with TIR sensor data. *European Journal of Remote Sensing*, *44*(1), 97–107. doi.org/10.5721/ItJRS20124418

Tepanosayn, G., Muradyan, V., Hovsepyan, A., Minasyan, L., Asmaryan, S. (2017). A Landsat 8 OLI Satellite Data-Based Assessment of Spatio-Temporal Variations of Lake Sevan Phytoplankton Biomass. In *Annals of Valahia University of Targoviste, Geographical Series* (Vol. 17, Issue 1, pp. 83–89). doi.org/10.1515/avutgs-2017-0008

Thomas, A., Byrne, D., Weatherbee, R. (2002). Coastal sea surface temperature variability from Landsat infrared data. *Remote Sensing of Environment*, *81*(2–3), 262–272. doi.org/10.1016/S0034-4257(02)00004-4

Wang, J., Rossow, W. B., Uttal, T., Rozendaal, M. (1999). Variability of cloud vertical structure during ASTEX observed from a combination of rawinsonde, radar, ceilometer, and satellite. *Monthly Weather Review*, *127*(10), 2484–2502. doi.org/10.1175/1520-0493(1999)127<2484:VOCVSD>2.0.CO;2

Xing, Q., Braga, F., Tosi, L., Lou, M., Wu, L., Tang, C., Zaggia, L., Teatini, P. (2014). *Towards Detecting Fresh Submarine Groundwater Discharge At the Laizhou Bay (Southern Bohai Sea, China) By Remote Sensing Methods*. *2014* (Nov.).

Xing, Q., Chen, C. Q., Shi, P. (2006). Method of integrating Landsat-5 and Landsat-7 data to retrieve sea surface temperature in coastal waters on the basis of local empirical algorithm. *Ocean Science Journal*, *41*(2), 97–104. doi.org/10.1007/BF03022414

Zhu, Z., Woodcock, C. E. (2012). Object-based cloud and cloud shadow detection in Landsat imagery. *Remote Sensing of Environment*, *118*, 83–94. doi.org/10.1016/j.rse.2011.10.028